

## Design of metalloporphyrins fused to imidazolium rings for binding DNA G-quadruplexes

Francesca Caporaletti<sup>a,†</sup>, Jenifer Rubio-Magnieto<sup>a,†</sup>, Mamadou Lo<sup>b,†</sup>, Jean-François Longevial<sup>b</sup>, Clémence Rose<sup>b</sup>, Sébastien Clément<sup>b</sup>, Arie van der Lee<sup>c</sup>, Mathieu Surin<sup>\*a</sup> and Sébastien Richeter<sup>\*b</sup>

<sup>a</sup>Laboratory for Chemistry of Novel Materials, Center of Innovation and Research in Materials and Polymers (CIRMAP), University of Mons-UMONS, Place du Parc 20, 7000 Mons, Belgium

<sup>b</sup>Institut Charles Gerhardt Montpellier, ICGM, UMR 5253, CNRS, Université de Montpellier, ENSCM, Place Eugène Bataillon, 34095 Montpellier Cedex 5, France

<sup>c</sup>Institut Européen des Membranes, IEM, UMR 5635, CNRS, Université de Montpellier, ENSCM, Place Eugène Bataillon, 34095 Montpellier Cedex 5, France

*Dedicated to Professor Atsuhiko Osuka on the occasion of his 65th birthday.*

Received 3 July 2019

Accepted 4 August 2019

**ABSTRACT:** Synthesis and characterization of nickel(II) *meso*-tetraarylporphyrins fused to imidazolium rings across  $\beta,\beta$ -pyrrolic positions and X-ray structure of the porphyrin where two opposed pyrrole units are fused to an imidazolium ring are presented. The interactions between these mono-, bis-, tris- and tetrakis(imidazolium) porphyrins with human telomeric DNA G-quadruplexes (G4) were investigated using UV-vis absorption spectroscopy, Circular Dichroism (CD) spectroscopy and Fluorescence Resonance Energy Transfer (FRET) melting assay. Possible binding modes between cationic porphyrins and a selected G4 sequence (d[AG<sub>3</sub>(T<sub>2</sub>AG<sub>3</sub>)<sub>3</sub>]), and relative stabilities of porphyrin/G4 complexes are discussed. Excepting porphyrins fused to one imidazolium ring, the other derivatives interact with G4 structures and their stabilization strongly depends on the porphyrin structure (number and localization of the imidazolium rings).

**KEYWORDS:** porphyrinoids, G-quadruplex, human telomeric DNA, circular dichroism spectroscopy, FRET melting assay.

\*Correspondence to: Sébastien Richeter, Institut Charles Gerhardt Montpellier, ICGM, UMR 5253, CNRS, Université de Montpellier, ENSCM, Place Eugène Bataillon, 34095 Montpellier Cedex 5 (France). tel.: +(33)467143971, email: sebastien.richeter@umontpellier.fr; Mathieu Surin, Laboratory for Chemistry of Novel Materials, University of Mons, Place du Parc 20, 7000 Mons, Belgium, email: mathieu.surin@umons.ac.be.

<sup>†</sup>Current address: F. Caporaletti: Department of Physics, Chemistry and Biology, Division of Chemistry, Linköping University, SE-58183 Linköping, Sweden & Institut Laue Langevin — LSS, 71 Avenue des Martyrs — CS 20156, 38042 Grenoble Cedex 9, France. Dr. J. Rubio-Magnieto: Bioinspired Supramolecular Chemistry and Materials group, Departament de Química Inorgànica i Orgànica, Universitat Jaume I, Avda Sos Baynat s/n, E-12071, Castelló, Spain. Dr. M. Lo: UFR des Sciences et Technologie, University Assane Seck de Ziguinchor, BP 523 Diabir — Ziguinchor — Sénégal.

## INTRODUCTION

Human telomeric DNA sequences d(TTAGGG)<sub>n</sub> are guanine-rich regions that can form intramolecular secondary four-strand structures called G-quadruplexes (G4) [1–3]. Four guanines are able to self-assemble through a network of Hoogsteen hydrogen bonds to form square-planar structures called G-quartets (Fig. 1a), and G4s are formed from G-quartets that stack on top of each other stabilized by alkali ions such as K<sup>+</sup> or Na<sup>+</sup> [4]. G4 can be found in telomeres, which are the regions at the end of chromosomes, and are supposed to play an important role in the cellular ageing processes [5]. Because they are also overrepresented in promoter regions of oncogenes [6], G4 structures have become potential biological targets for developing new treatments against cancer [7–9]. For

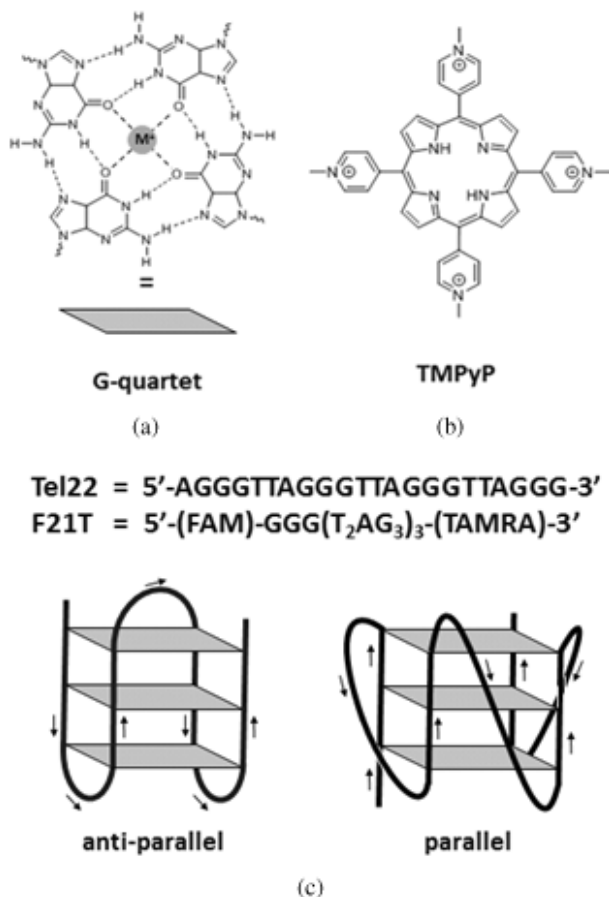


**Fig. 1.** Structures of a G-quartet with  $M = \text{Na}^+$  or  $\text{K}^+$  (a) and **TMPyP** (b) Sequence and possible folding topologies of **Tel22** and **F21T** (c)

this purpose, molecules able to bind and stabilize G4 are actively investigated to inhibit oncogenes expression, but the large structural polymorphism of G4 and the low level of understanding of their interactions with synthetic molecules have greatly hampered the development of this type of treatment. Flat  $\pi$ -conjugated macrocycles such as porphyrins are known to interact with G4, and different structural features like the nature of the peripheral groups on the porphyrin core or the nature of the metal in the cavity will play significant roles on the binding modes with G4 [8]. For example, free-base porphyrins or those containing flat square-planar metal complexes are able to intercalate in between G-quartets. In contrast, metalloporphyrins containing axial ligands preferentially bind externally to G4. Cationic porphyrins are preferentially investigated as G4 ligands because the positive charges dramatically improve water solubility and favor electrostatic interactions with the negatively charged DNA [10–19]. The tetrakis(*N*-methylpyridinium-4-yl)porphyrin (**TMPyP**, Fig. 1b) was extensively studied and is the archetype of porphyrins able to bind and stabilize G-quadruplexes by different interactions like  $\pi$ -stacking interactions with square-planar G quartets

and/or electrostatic interactions with the phosphate groups of DNA [11–19].

While positive charges of **TMPyP** are located on the four *meso* pyridinium groups, we propose here to investigate a new family of G4 ligands which are nickel(II) porphyrins fused to imidazolium salts **1**, **2-trans**, **2-cis**, **3** and **4** (Chart 1). The original structural aspect of these compounds is that positive charges are located on the aromatic cores of these  $\pi$ -extended porphyrins. UV-vis absorption spectroscopy and Circular Dichroism (CD) spectroscopy were performed in aqueous solutions to investigate interactions between **Tel22**, the selected G-rich DNA sequence ( $d[\text{AG}_3(\text{T}_2\text{AG}_3)_3]$ ) depicted in Fig. 1c, and cationic metalloporphyrins: **1**, **2-trans**, **2-cis**, **3** and **4**. Fluorescence Resonance Energy Transfer (FRET) melting assays were also performed with sequence **F21T**, depicted in Fig. 1c, to provide information on the stabilization of G4 by porphyrins fused to imidazolium salts. In addition, the X-ray structure of the nickel(II) porphyrin **2-trans** is also presented.

## RESULTS AND DISCUSSION

### Synthesis and characterization of metalloporphyrins fused to imidazolium salts

The synthesis of porphyrins fused to imidazole rings across their  $\beta, \beta'$ -pyrrolic positions, namely **mono(imidazole)**, **bis(imidazole)-trans**, **bis(imidazole)-cis**, **tris(imidazole)** and **tetrakis(imidazole)** was previously reported in the literature [20, 21]. The imidazolium salts **1**, **2-trans**, **2-cis**, **3** and **4** were obtained by alkylating the corresponding imidazole derivatives with an excess of iodomethane (Chart 1) [14, 16]. All compounds were characterized by mass spectrometry and correct mass peaks were observed for these cationic species at  $m/z = 963.46$  (**1**),  $516.25$  (**2-trans**),  $516.25$  (**2-cis**),  $367.18$  (**3**) and  $292.65$  (**4**) in good agreement with their calculated values.  $^1\text{H}$  NMR spectra of porphyrins **1**, **2-trans**, **2-cis** and **3** were sharp and well resolved in  $\text{CDCl}_3$ . The protons of the imidazolium rings could be observed at  $\delta \sim 10\text{--}11$  ppm in good agreement with what is usually observed by  $^1\text{H}$  NMR spectroscopy for imidazolium salts containing  $I^-$  as a counter anion in non-coordinating solvents. Methyl groups of the imidazolium rings were observed at  $\delta \sim 3.00\text{--}3.20$  ppm. As expected, tetracationic species **4** is not soluble in chlorinated solvents. Therefore,  $^1\text{H}$  NMR spectroscopy was performed in a polar solvent such as  $\text{CD}_3\text{OD}$ , leading to broad and split signals. This can be explained by the fact that the four electron-deficient imidazolium rings favor axial coordination on nickel(II) and that the resulting square pyramidal and/or octahedral distorted nickel(II) porphyrins are paramagnetic species ( $S = 1$ ). The same phenomenon was observed in the  $^1\text{H}$  NMR spectrum of porphyrin **3**, which was also soluble in  $\text{CD}_3\text{OD}$  [22].

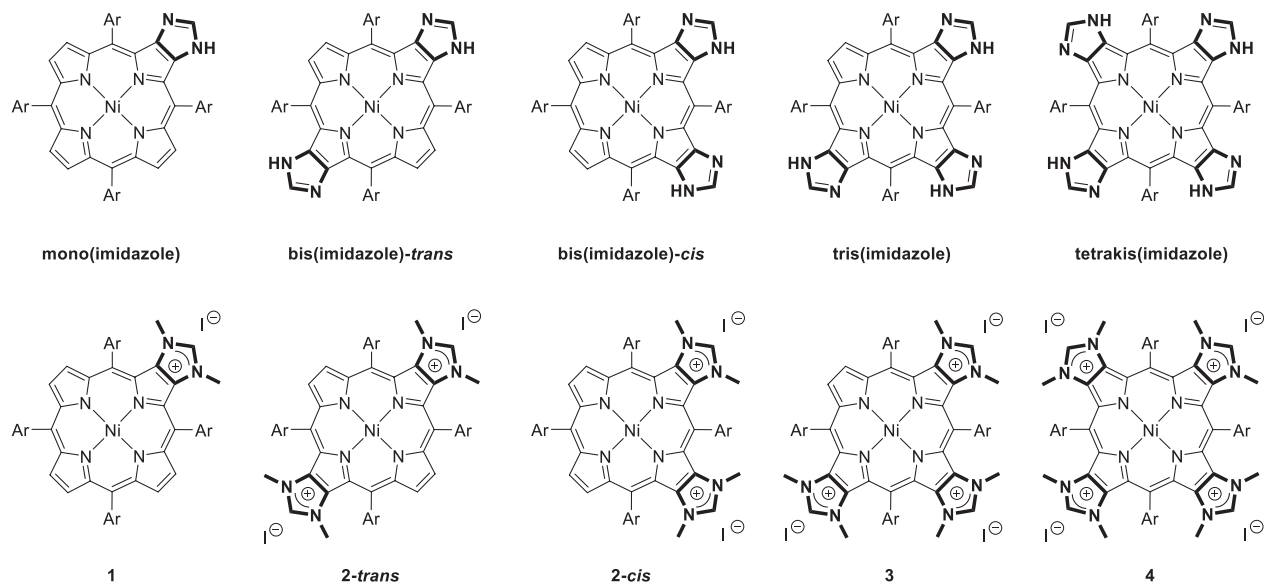


**Chart 1.** Structures of the nickel(II) porphyrins studied here (Ar = 4-*t*BuPh)

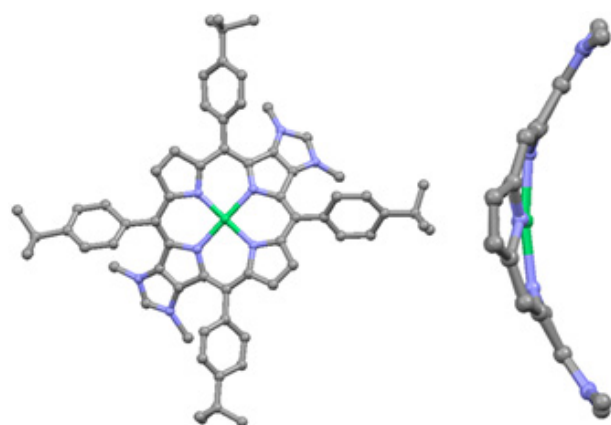


**Fig. 2.** X-ray structure of the nickel(II) porphyrin **2-trans**. (solvent, iodide and hydrogen atoms omitted for clarity). Left: top view showing the functionalization of the two opposed pyrrole rings. Right: side view showing the saddle-shaped distortion of the porphyrin core (*meso* aryl groups omitted for clarity)

We could obtain single crystals suitable for an X-ray diffraction study of the dicationic porphyrin **2-trans** confirming that two opposed pyrroles are fused to imidazolium rings (Fig. 2). The nickel(II) ion adopts a slightly distorted square-planar geometry ( $170^\circ < \text{N-Ni-N}$  angles  $< 172^\circ$ ). The two Ni–N distances where N atoms belong to the pyrroles fused to imidazolium rings are equal to  $\sim 1.99$  Å and are longer compared to the two other Ni–N distances (1.81–1.90 Å). As can be seen in Fig. 2 (right side), the imidazolium rings and their corresponding fused pyrroles are coplanar. A very strong saddle-shaped distortion is also observed

for the porphyrin core with maximum displacements of 1.03–1.06 Å for the four C $\beta$  atoms fused to the two imidazolium rings and an average displacement of  $\sim 0.50$  Å for the core atoms with respect to the porphyrin mean plane (based on a least-squares plane calculated for the 24 core atoms of the porphyrin). The nickel(II) cation is perfectly located in the porphyrin mean plane. Because of the porphyrin core saddle-shaped conformation, the two imidazolium rings are located on the same side of the porphyrin mean plane with maximum displacements of 2.15–2.18 Å for the two C atoms between the two N atoms. This very strong saddle-shaped distortion observed for porphyrin **2-trans** is in good agreement with previous studies showing that increasing the steric demand of peripheral substituents gradually increases the degree of non-planarity of the porphyrin core [23, 24].

### UV-vis absorption and circular dichroism spectroscopies

To investigate binding properties of nickel(II) porphyrins **1**, **2-trans**, **2-cis**, **3** and **4** to human telomeric G4, we used human telomeric DNA sequence d[AG<sub>3</sub>(T<sub>2</sub>AG<sub>3</sub>)<sub>3</sub>], namely **Tel22**, as a model sequence. **Tel22** adopts different G4 structures according to the nature of the alkali cation in the aqueous solutions. In the presence of Na<sup>+</sup>, **Tel22** adopts an anti-parallel “basket-type” structure (Fig. 1c) [25]. In the presence of K<sup>+</sup>, **Tel22** presents a mixture of anti-parallel and parallel structures, which are in a dynamic equilibrium (Fig. 1c) [26–29]. Because G4 are chiral species, they can be analyzed by CD spectroscopy. Indeed, the CD spectrum of **Tel22** in an aqueous solution containing Na<sup>+</sup> is characterized by an intense negative peak at 260 nm followed by a positive peak at 300 nm. Meanwhile, in an aqueous

solution containing  $K^+$ , **Tel22** exhibits a CD spectrum characterized by a positive maximum at 290 nm and a minute plateau at 270 nm. The molecular interactions between nickel(II) porphyrins fused to imidazolium salts depicted in Chart 1 and **Tel22** were investigated by combining CD and UV-vis absorption spectroscopy. Porphyrins are achiral molecules and they do not present CD signals in their Soret absorption bands. However, when porphyrins interact with chiral species like G4, the obtained complex becomes chiral and produces an induced CD (ICD) signal when the  $\pi$  system of the porphyrin is in close proximity of G4 [30]. Depending on the interaction modes between porphyrins and G4, different ICD signals can be observed in the Soret absorption band of porphyrins: intercalation and external binding are characterized by negative and positive ICD signals, respectively. End-stacking interactions between porphyrins and G4 are usually characterized by split bisignate ICD signals [31–33].

As previously reported, porphyrin **4**, which is fused to four imidazolium rings, interacts with **Tel22**, adopting anti-parallel ( $Na^+$ ) and parallel ( $K^+$ ) conformations [22]. In both cases, negative ICD signals could be observed in the Soret absorption band of porphyrin **4** upon increasing the molar ratio of porphyrin **4**/**Tel22** up to 5:1 (Fig. S13). This is a good indication that porphyrin **4** interacts with **Tel22**. However, these porphyrins are strongly saddle-shaped as illustrated by the X-ray diffraction analysis and computational studies and, as a consequence their

intercalation between G-quartets is very unlikely. For this reason, molecular dynamics simulations were previously carried out to provide insights into possible binding modes of porphyrin **4** to anti-parallel and parallel G4 [22]. With anti-parallel G4, two preferential binding modes were determined. One binding mode occurs at the bottom of anti-parallel G4 with two parallel d(TTA) loops, because saddle-shaped porphyrin **4** perfectly accommodates the d(TTA) loop structures and the two opposed cationic imidazolium groups strongly interact with negatively charged phosphate groups. External binding modes in the wide groove of anti-parallel G4 involving  $\pi$ -stacking interactions were also observed. With parallel G4, top and bottom G-quartets are not sterically hindered by loops. As a consequence, one preferential binding mode is due to partial end-stacking between porphyrin **4** and the top accessible G-quartet.

Following this study, we decided to investigate the binding properties of other cationic nickel(II) porphyrins depicted in Chart 1. We observed that the nickel(II) porphyrin **3** presents strong binding abilities with **Tel22**. Indeed, in porphyrin **3**/**Tel22** mixtures prepared in the presence of  $Na^+$ , a strong bisignate (-/+) ICD signal in the Soret absorption band of porphyrin **3** could be observed at a porphyrin **3**/**Tel22** molar ratio of 3:1, in agreement with end-stacking interaction with anti-parallel G4 (Fig. 3a). Similar behavior was observed between porphyrin **3** and **Tel22** in the presence of  $K^+$  (Fig. 3b).

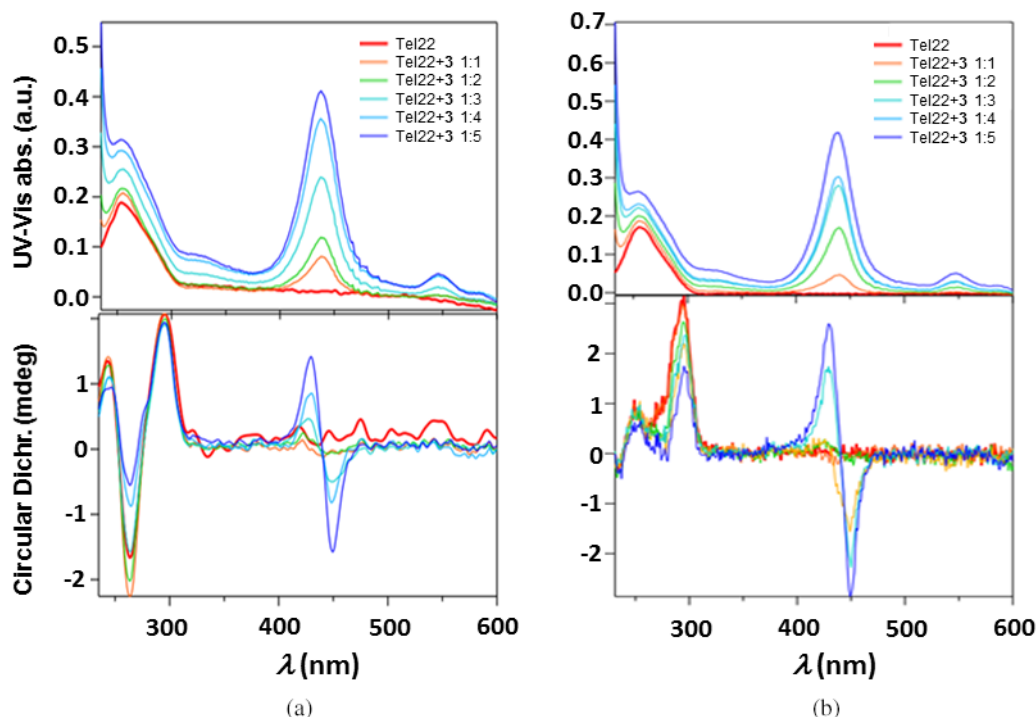


**Fig. 3.** UV-vis absorption (top) and CD (bottom) spectra of porphyrin **3**/**Tel22** mixtures in TE buffer + 100 mM NaCl (a) and in TE buffer + 100 mM KCl (b)

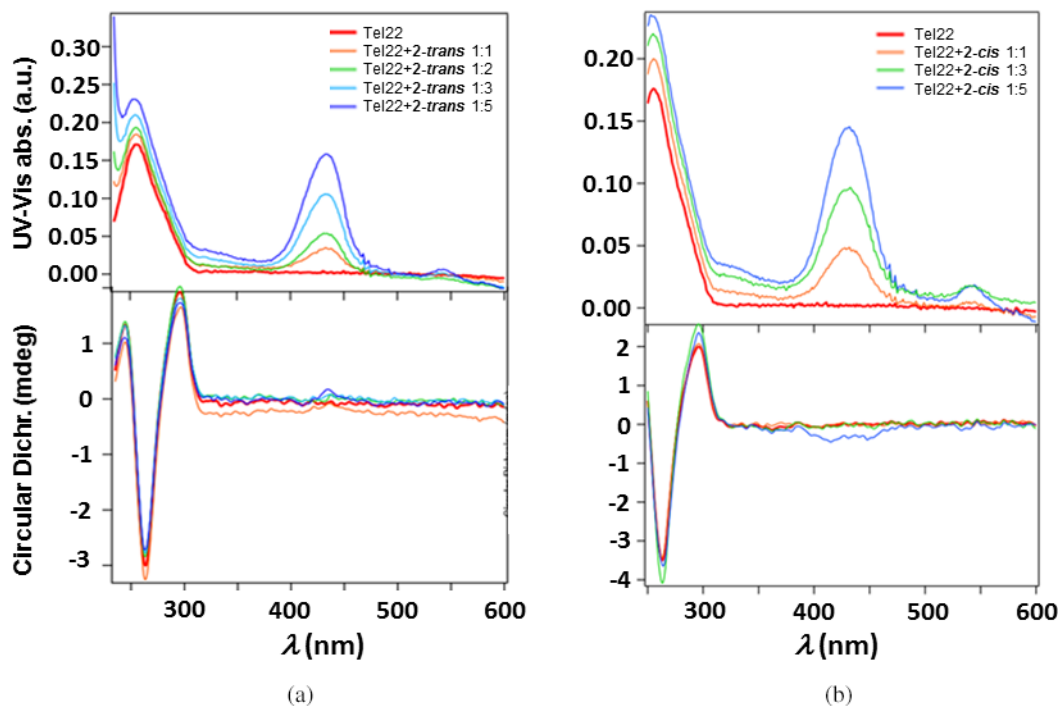


**Fig. 4.** UV-vis absorption (top) and CD (bottom) spectra of porphyrin **2-trans**/Tel22 (a) and porphyrin **2-cis**/Tel22 (b) mixtures in TE buffer + 100 mM NaCl

Then, we compared the binding properties of the two isomeric porphyrins **2-trans** and **2-cis** with Tel22. Mixtures of **2-trans** and Tel22 were first prepared in the presence of Na<sup>+</sup> and a weak positive ICD signal could be observed in the Soret absorption band of porphyrin **2-trans** at a **2-trans**/Tel22 molar ratio of 5:1, with only slight modifications of the CD signals of Tel22 (Fig. 4a). Interestingly, the two porphyrins **2-trans** and **2-cis** present different binding modes towards anti-parallel G4 because the two ICD signals are opposite at this molar ratio: positive for porphyrin **2-trans** (Fig. 4a) and negative for porphyrin **2-cis** (Fig. 4b). In the presence of K<sup>+</sup> and Tel22 adopting a parallel G4 structure in these conditions, no ICD signal in the Soret absorption band of **2-trans** could be observed for **2-trans**/Tel22 up to a molar ratio of 5:1 (Fig. 5a). In contrast, with porphyrin **2-cis**/Tel22 mixtures, a bisignate (-/+) ICD signal appeared in the Soret absorption band of **2-cis** at a low molecular ratio of 1:1, similar to the one observed with porphyrin **3** (Fig. 5b). This ICD signal became negative at a porphyrin **2-cis**/Tel22 molar ratio of 5:1, suggesting a possible phase transition between binding modes. A significant decrease in the CD signals of Tel22 could also be observed and may be due to the possible unfolding of G4 conformations when porphyrin **2-cis** was used in excess. This behavior, which was also observed with other cationic porphyrins, may likely be due to stronger intermolecular interactions of porphyrins **2-trans** and **2-cis** with DNA bases [34, 35].

Finally, we observed in mixtures of monocationic porphyrin **1** and Tel22 that there is no ICD signal in the

Soret absorption band of porphyrin **1** in the presence of Na<sup>+</sup> or K<sup>+</sup> (Fig. S14). This and the fact that CD bands of Tel22 are barely modified in porphyrin **1**/Tel22 mixtures suggest that no or very weak interactions exist between monocationic porphyrin **1** and Tel22 and that porphyrin **1** is not a good ligand to bind and stabilize this selected G4 sequence.

### FRET melting studies

Fluorescence Resonance Energy Transfer (FRET) melting study is a valuable method to determine the stabilization of the porphyrins towards G4 [36, 37]. This method is based on determining the melting properties of the oligonucleotide by fluorescence spectroscopy. For this purpose, we used a human telomeric sequence named **F21T**, which is end-capped with a fluorescein amidite dye (FAM) and tetramethylrhodamine (TAMRA) at the extremity 5' and 3', respectively. This labelled oligonucleotide 5'-(FAM)-GGG(T<sub>2</sub>AG<sub>3</sub>)<sub>3</sub>-(TAMRA)-3' is able to adopt G4 conformations in aqueous solutions containing alkali cations. TAMRA quenches the emission of FAM in **F21T** adopting G4 conformations because of their close proximity [22]. Emission of FAM increases upon heating because of the longest distance between the dyes due to G4 denaturation. Unfolding can be followed by plotting the increase of FAM fluorescence as a function of temperature, and half-melting temperatures ( $T_{1/2}$ ) can be obtained by Hill equation fit. Stabilization of G4 by the different porphyrins can be quantified by determining half-melting temperature differences  $\Delta T_{1/2}$  between **F21T**

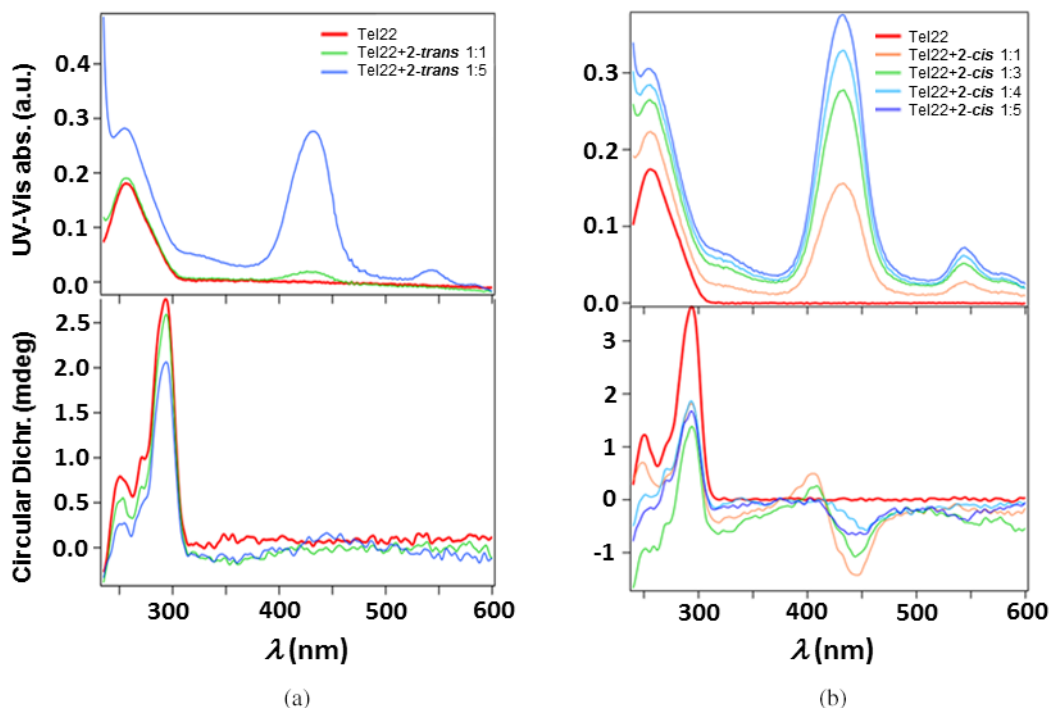


**Fig. 5.** UV-vis absorption (top) and CD (bottom) spectra of porphyrin **2-trans**/Tel22 (a) and porphyrin **2-cis**/Tel22 (b) mixtures in TE buffer + 100 mM KCl

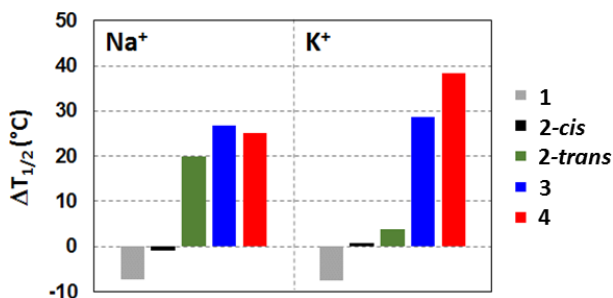


**Fig. 6.** Melting temperature differences  $\Delta T_{1/2}$  from FRET melting assays with porphyrin/F21T in a 5:1 molar

and porphyrin/F21T mixtures ( $\Delta T_{1/2} = T_{1/2(\text{porphyrin}/\text{F21T})} - T_{1/2(\text{F21T})}$ ). FRET melting studies are interesting in the present case, because fluorescence spectroscopy is a more sensitive technique compared to UV-vis absorption and CD spectroscopies. Indeed, FRET melting studies allowed us to use very low concentrations of sequence **F21T** (200 nM) and porphyrins **1–4** (up to 1  $\mu\text{M}$ ), thus limiting the risk of aggregation of porphyrins **1–3** which are less soluble in aqueous media compared to porphyrin **4**.

The obtained data are summarized in Fig. 6. In aqueous solutions containing  $\text{Na}^+$  and porphyrin/F21T mixtures at porphyrin/F21T up to a 5:1 molar ratio, we observed that porphyrins **4** ( $\Delta T_{1/2} = +25.0^\circ\text{C}$ ), **3** ( $\Delta T_{1/2} = +26.8^\circ\text{C}$ ) and **2-trans** ( $\Delta T_{1/2} = +19.8^\circ\text{C}$ ) are able to stabilize anti-parallel G4 structures. The common structural feature between these three porphyrin derivatives is the presence of two opposed imidazolium units which are on the same side

with respect to the porphyrin mean plane. As previously showed by molecular dynamics simulations, one binding mode of porphyrin **4** occurs at the bottom of anti-parallel G4 between negatively charged phosphate groups of the two parallel d(TTA) loops and the two opposed cationic imidazolium groups [22]. We presume that similar interactions are possible with porphyrins **3** and **2-trans**. Interestingly, such interactions are not possible with porphyrin **2-cis**, which has two adjacent imidazolium units located above and underneath with respect to the porphyrin mean plane. This can explain why porphyrin **2-cis** is not able to stabilize anti-parallel G4 structures ( $\Delta T_{1/2} = -0.9^\circ\text{C}$ ). In aqueous solutions containing  $\text{K}^+$ , both porphyrins **3** and **4** efficiently stabilized parallel G4 conformation, but the opposite effect was observed as the stabilization of G4 was improved with porphyrin **4** ( $\Delta T_{1/2} = +38.5^\circ\text{C}$ ) compared to porphyrin **3** ( $\Delta T_{1/2} = +28.6^\circ\text{C}$ ). On the contrary, neither isomeric porphyrin **2-trans** nor porphyrin **2-cis** are able to stabilize G4 structures ( $\Delta T_{1/2} = +3.8$  and  $+0.8^\circ\text{C}$ , respectively). The negative values of  $\Delta T_{1/2}$  determined for porphyrin **1**/F21T mixtures at a 5:1 molar ratio in the presence of  $\text{Na}^+$  ( $-7.2^\circ\text{C}$ ) or  $\text{K}^+$  ( $-7.5^\circ\text{C}$ ) show that this monocationic porphyrin destabilizes G4 conformations.

## EXPERIMENTAL

### General

All chemicals were purchased from the usual commercial sources and used as received. Reactions were

performed under argon using oven-dried glassware and Schlenk techniques. Dry DMF was obtained by a solvent purification system, PureSolve MD5, from Innovative Technology. Preparative purifications were performed by silica gel flash column chromatography (Merck@ 40–60  $\mu\text{M}$ ). Solvents used as eluents are technical grade.  $^1\text{H}$  and  $^{13}\text{C}\{^1\text{H}\}$  NMR spectra were recorded on a Bruker 200 or 500 MHz spectrometer.  $^1\text{H}$  and  $^{13}\text{C}\{^1\text{H}\}$  NMR spectra were calibrated to TMS on the basis of the relative chemical shift of the solvent as an internal standard. Abbreviations used for  $^1\text{H}$  NMR spectra are as follow: s singlet, d doublet. UV-vis absorption spectra were recorded in  $\text{CH}_2\text{Cl}_2$  with a JASCO V-750 UV-vis spectrophotometer in quartz cells of 10 mm (Hellma). High-resolution mass spectra (HRMS) were recorded on MALDI-TOF and ESI-TOF Q instruments in positive mode (see Figs S1–S12).

### Synthesis of porphyrin derivatives

Nickel(II) porphyrins **mono(imidazole)**, **bis(imidazole)-trans**, **bis(imidazole)-cis**, **tris(imidazole)** and **tetrakis(imidazole)** were synthesized following procedures described in Refs. [20] and [21].

**Porphyrin 1.** Porphyrin fused to one imidazolium salt, **1**, was synthesized from porphyrin **mono(imidazole)** following procedure described in Ref. [20].

**Porphyrin 2-trans.** Porphyrin **bis(imidazole)-trans** (120 mg, 0.12 mmol) was dissolved in DMF (20 mL). Then,  $\text{K}_2\text{CO}_3$  (34 mg, 0.24 mmol) and iodomethane (10 mL, large excess) were added and the reaction mixture was stirred at room temperature for 48 h. Afterwards, DMF was evaporated under reduced pressure and the crude material was purified by chromatography ( $\text{SiO}_2$ , eluent from  $\text{CH}_2\text{Cl}_2$  to  $\text{CH}_2\text{Cl}_2/\text{CH}_3\text{OH}$  95:5). The red band was isolated and the solvent was evaporated. Crystallization from  $\text{CH}_2\text{Cl}_2/n$ -hexane afforded porphyrin **2-trans** as a red powder. Yield 146 mg (95%). UV-vis ( $\text{CH}_2\text{Cl}_2$ )  $\lambda_{\text{max}}$ , nm (log  $\epsilon$ ) 432 (5.4), 542 (4.2), 580 sh (3.8).  $^1\text{H}$  NMR (200 MHz,  $\text{CDCl}_3$ , 298 K)  $\delta$  1.56 (s, 36H, *t*Bu), 3.17 (s, 12H, N- $\text{CH}_3$ ), 7.86 (d,  $^3J_{\text{H-H}} = 8.2$  Hz, 8H, Ar), 8.12 (d,  $^3J_{\text{H-H}} = 8.2$  Hz, 8H, Ar), 8.57 (s, 4H, pyrrole-*H*), 10.72 (s, 2H, imidazolium-*H*) ppm.  $^{13}\text{C}\{^1\text{H}\}$  NMR (125.8 MHz,  $\text{CD}_2\text{Cl}_2$ , 298 K)  $\delta$  31.6, 35.5, 36.3, 118.9, 126.2, 128.6, 133.8, 135.5, 136.8, 139.0, 145.1, 147.0, 154.3 ppm. MS (ESI-TOF)  $m/z$  516.2545 (calcd for  $[\text{M} - 2\text{I}]^{2+}$  516.2533).

**Porphyrin 2-cis.** Porphyrin **bis(imidazole)-cis** (150 mg, 0.15 mmol) was dissolved in DMF (20 mL). Then,  $\text{K}_2\text{CO}_3$  (43 mg, 0.31 mmol) and iodomethane (10 mL, large excess) were added and the reaction mixture was stirred at room temperature for 48 h. Afterwards, DMF was evaporated under reduced pressure and the crude material was purified by chromatography ( $\text{SiO}_2$ , eluent from  $\text{CH}_2\text{Cl}_2$  to  $\text{CH}_2\text{Cl}_2/\text{CH}_3\text{OH}$  95:5). The red band was isolated and the solvent was evaporated. Crystallization from  $\text{CH}_2\text{Cl}_2/n$ -hexane

afforded porphyrin **2-cis** as a red powder. Yield 180 mg (90%). UV-vis ( $\text{CH}_2\text{Cl}_2$ )  $\lambda_{\text{max}}$ , nm (log  $\epsilon$ ) 433 (5.3), 542 (4.2), 578 sh (3.7).  $^1\text{H}$  NMR (200 MHz,  $\text{CDCl}_3$ , 298 K)  $\delta$  1.55 (s, 18H, *t*Bu), 1.57 (s, 9H, *t*Bu), 1.62 (s, 9H, *t*Bu), 3.02 (s, 6H, N- $\text{CH}_3$ ), 3.15 (s, 6H, N- $\text{CH}_3$ ), 7.78 (d,  $^3J_{\text{H-H}} = 8.2$  Hz, 2H, Ar) 7.86 (d,  $^3J_{\text{H-H}} = 8.2$  Hz, 4H, Ar), 7.98 (d,  $^3J_{\text{H-H}} = 8.2$  Hz, 2H, Ar), 8.01 (d,  $^3J_{\text{H-H}} = 8.2$  Hz, 2H, Ar), 8.13 (d,  $^3J_{\text{H-H}} = 8.2$  Hz, 4H, Ar), 8.26 (d,  $^3J_{\text{H-H}} = 8.3$  Hz, 2H, Ar), 8.63 (s, 4H, pyrrole-*H*), 10.77 (s, 2H, imidazolium-*H*) ppm.  $^{13}\text{C}\{^1\text{H}\}$  NMR (125.8 MHz,  $\text{CD}_2\text{Cl}_2$ , 298 K)  $\delta$  31.6, 31.6, 31.7, 35.3, 35.5, 35.7, 36.1, 36.2, 114.4, 119.0, 123.3, 125.1, 126.2, 127.7, 128.1, 128.6, 133.5, 133.6, 134.8, 135.8, 135.9, 136.3, 136.7, 137.3, 138.8, 139.2, 145.1, 147.4, 147.7, 152.3, 154.2, 156.1 ppm. MS (MALDI-TOF)  $m/z$  516.2532 (calcd for  $[\text{M} - 2\text{I}]^{2+}$  516.2533).

**Porphyrin 3.** Porphyrin **tris(imidazole)** (50 mg, 0.05 mmol) was dissolved in DMF (15 mL). Then,  $\text{K}_2\text{CO}_3$  (21 mg, 0.15 mmol) and iodomethane (5 mL, large excess) were added and the reaction mixture was stirred at room temperature for 48 h. Afterwards, DMF was evaporated under reduced pressure and the crude material was purified by chromatography ( $\text{SiO}_2$ , eluent from  $\text{CH}_2\text{Cl}_2$  to  $\text{CH}_2\text{Cl}_2/\text{CH}_3\text{OH}$  95:5). The red band was isolated and the solvent was evaporated. Crystallization from  $\text{CH}_2\text{Cl}_2/n$ -hexane afforded porphyrin **3** as a red powder. Yield 53 mg (73%). UV-vis ( $\text{CH}_2\text{Cl}_2$ )  $\lambda_{\text{max}}$ , nm (log  $\epsilon$ ) 438 (5.4), 547 (4.3), 580 (3.8).  $^1\text{H}$  NMR (200 MHz,  $\text{CDCl}_3$ , 298 K)  $\delta$  1.51 (s, 18H, *t*Bu), 1.53 (s, 18H, *t*Bu), 2.94 (2s, 12H, N- $\text{CH}_3$ ), 3.06 (s, 6H, N- $\text{CH}_3$ ), 7.85 (d,  $^3J_{\text{H-H}} = 7.9$  Hz, 4H, Ar), 7.93 (d,  $^3J_{\text{H-H}} = 7.9$  Hz, 4H, Ar), 8.09 (d br,  $^3J_{\text{H-H}} = 7.9$  Hz, 4H, Ar), 8.24 (d,  $^3J_{\text{H-H}} = 7.9$  Hz, 4H, Ar), 8.58 (s, 2H, pyrrole-*H*), 10.68 (s, 1H, imidazolium-*H*), 10.82 (s, 2H, imidazolium-*H*) ppm.  $^{13}\text{C}\{^1\text{H}\}$  NMR (125.8 MHz,  $\text{CD}_2\text{Cl}_2$ , 298 K)  $\delta$  31.7, 31.8, 35.6, 35.9, 36.3, 36.3, 36.3, 116.4, 120.9, 126.4, 126.6, 127.4, 127.8, 128.0, 130.8, 131.0, 131.6, 135.4, 136.0, 136.4, 140.9 (broad), 145.4, 146.1, 146.3, 150.3, 154.8, 156.5 ppm. MS (MALDI-TOF)  $m/z$  367.1849 (calcd for  $[\text{M} - 3\text{I}]^{3+}$  367.1838).

**Porphyrin 4.** Porphyrin fused to one imidazolium salt **4** was synthesized from porphyrin **tetrakis(imidazole)** following procedure described in Ref. [22].

### X-ray diffraction analysis

A Rigaku Oxford-Diffraction Xcalibur-1 diffractometer with sealed-tube Mo- $\text{K}\alpha$  radiation was used for the data collection. The CrysAlis Pro program [38] was employed for the integration of the data using default parameters for the empirical absorption correction using spherical harmonics on symmetry-equivalent and redundant data and correcting for Lorentz and polarization effects. The *ab-initio* iterative charge flipping method was used to solve the crystal structure with parameters described elsewhere [39] with the Superflip program [40] and refined using full-matrix

least-squares procedures on structure factor amplitudes  $F$  as implemented in CRYSTALS [41] using all independent reflections with  $I > 2\sigma(I)$ . Hydrogen atoms were refined with riding constraints. The data collected appeared to be very weak, so weak that it was decided to cut them at 1.0 Å resolution during the data integration. In order to cope with the low reflections-to-parameter ratio, only the heavy atoms (Ni and I) were refined anisotropically. Due to the low data quality, the results of the refinements are not very good with  $R_1$  agreement factors of 0.1307. Despite the moderate data quality, the final structure is of acceptable quality and there is no doubt that the final structure is correct with respect to its molecular geometry (Fig. S15 in ESI). Crystal data of nickel(II) porphyrin **2-trans** (Table S1): formula  $C_{69}H_{71}Cl_9I_2N_8Ni$ , moiety  $C_{66}H_{68}N_8Ni^{2+}$ , 2(I), 3(CHCl<sub>3</sub>),  $M = 1643.88 \text{ g}\cdot\text{mol}^{-1}$ , crystal size  $0.02 \times 0.04 \times 0.08 \text{ mm}$ , monoclinic, space group  $P2_1/n$ ,  $a = 15.699 (3) \text{ \AA}$ ,  $b = 21.704 (2) \text{ \AA}$ ,  $c = 23.178 (4) \text{ \AA}$ ,  $\alpha = 90^\circ$ ,  $\beta = 107.637 (19)^\circ$ ,  $\gamma = 90^\circ$ ,  $V = 7526.2 (12) \text{ \AA}^3$ ,  $Z = 4$ ,  $\rho_{\text{calc}} = 1.451 \text{ Mg/m}^3$ ,  $T = 175 \text{ K}$ ,  $\theta_{\text{max}} = 20.815^\circ$ , 16783 reflections measured, 7851 unique reflections,  $R_1 = 0.1307$ ,  $wR_2 = 0.1402$ , GoF = 0.8374. CCDC N° 1943641.

### Preparation of porphyrin/Tel22 mixtures

Oligonucleotides (ODNs) **Tel22** (d[AG<sub>3</sub>(T<sub>2</sub>AG<sub>3</sub>)<sub>3</sub>]) and **F21T** (5'-FAM-GGG(T<sub>2</sub>AG<sub>3</sub>)<sub>3</sub>-TAMRA-3') were obtained from Eurogentec (Belgium) with the highest purity grade (UltraPureGold). ODNs were dissolved at a concentration of 100 μM in TE buffer (10 mM Tris buffer and 1 mM EDTA in MilliQ water) at pH 7.4. The solutions were centrifuged for 2 min at 2000 rpm. Small volumes of this solution were used in order to prepare different aliquots, on which were added TE buffer, or TE buffer + KCl 3M or + NaCl 3M in order to obtain solutions in pure TE buffer, TE buffer + 100 mM K<sup>+</sup>, or TE buffer + 100 mM Na<sup>+</sup> ions, respectively. The final solution was mixed using a vortex. The concentration of the aliquot of DNA in the buffer solution was determined by using UV-vis absorption spectroscopy at 25 °C using the specific extinction coefficients at 260 nm ( $\epsilon_{260}$ ) of **Tel22**, which is 228 500 L·mol<sup>-1</sup>·cm<sup>-1</sup>. The nickel(II) porphyrins samples were dissolved in TE buffer (pH 7.4, 10 mM Tris buffer and 1 mM EDTA) + 100 mM KCl or NaCl using a small proportion of DMSO (1 mM), and the molar ratio between metalloporphyrins and DNA was adjusted using the calculated molar concentrations of ODN (around 3.5 μM). The solutions of metalloporphyrins and ODN were mixed and stirred using a vortex at vigorous speed for 2 min and allowed to equilibrate for 30 min.

### UV-vis and circular dichroism spectroscopies

UV-vis absorption and circular dichroism (CD) measurements were recorded using a Chirascan™ Plus CD Spectrophotometer from Applied Photophysics. The measurements were carried out using 1 mm suprasil

quartz cells from Hellma Analytics. The spectra were recorded between 200 and 650 nm, with a bandwidth of 1 nm, time per point 1 s and 2 repetitions. The buffered water solvent reference spectra were used as baselines and were automatically subtracted from the CD spectra of the samples.

### FRET melting assays

FRET melting assays were performed according to the procedure described in Ref. [37], using a double-dye labelled ODN 5'-FAM-GGG(T<sub>2</sub>AG<sub>3</sub>)<sub>3</sub>-TAMRA-3' (**F21T**) from Eurogentec, Belgium. The solutions were prepared at a concentration of around 200 nM (base concentration) in 10 mM lithium cacodylate buffer (pH = 7.2) in presence of 10 mM KCl + 90 mM LiCl (K<sup>+</sup> medium). A first heating/cooling cycle of **F21T** in buffer was carried out to form the G4 secondary structure. The nickel(II) porphyrins under study were then added at a concentration of ~1 μM, and the mixture was equilibrated at 25 °C during 5 min. The FRET spectra were measured using a Chirascan™ Plus instrument equipped for fluorescence measurements. The samples were excited at 492 nm and the fluorescence emission spectra were collected between 500 and 700 nm. The temperature was varied with a stepped ramping from 10 °C to 94 °C, at a slow rate (step of 0.5 °C and 2 min per step). The melting of the **F21T** (the unfolding of G4) was monitored by measuring the fluorescence of FAM at 516 nm. The FAM emission intensity was normalized and the half-melting temperature  $T_{1/2}$  was obtained from fitting the curve with a Hill equation.

## CONCLUSION

The synthesis of nickel(II) porphyrins fused to imidazolium rings was achieved by alkylating the corresponding porphyrins equipped with imidazole groups. These cationic porphyrins were investigated as potential ligands able to bind and stabilize human telomeric DNA G-quadruplexes. Data obtained from CD spectroscopy and FRET melting assays show that nickel(II) porphyrins fused to three and four imidazolium rings bind and efficiently stabilize G4 structures in both parallel and anti-parallel conformations. Interestingly, both isomeric porphyrins with two adjacent or two opposed imidazolium rings present different binding properties. We observed that the isomer with two opposed imidazolium rings, namely porphyrin **2-trans**, can efficiently stabilize anti-parallel G4 structures, whereas this is not the case for porphyrin **2-cis** with two adjacent imidazolium rings. This is probably due to more favorable interactions between DNA and imidazolium rings located on the same side of the porphyrin mean plane due to the saddle-shaped distortion of the macrocycle. The two porphyrins with one or two adjacent imidazolium rings do not stabilize G-quadruplex structures. Our

future studies will be devoted to investigating the effect of the inner metal ions of these cationic porphyrins on their ability to bind and stabilize human telomeric DNA G-quadruplexes.

### Acknowledgments

The authors are grateful to the University of Montpellier, the CNRS and the French Ministry of Research for financial support. SR is also grateful for financial support from the Région Languedoc-Roussillon (Research Grant “Chercheur(se)s d’Avenir – 2015-005984) and the FEDER program (Fonds Européen de Développement Régional). ML is grateful to the Agence Nationale de la Recherche (ANR) for financial support (research project ANR-09-JCJC-0089-01). Research in Mons was supported by the University of Mons and the Fund for Scientific Research (F.R.S.-FNRS) under the grants No. F.4532.16 (MIS SHERPA) and No. 1.B333.15F (CHIRNATES). J.R.M. and M.S. are F.R.S.-FNRS researchers.

### Supporting information

Figures S1–S15 and Table S1 are given in the supplementary material. This material is available free of charge via the Internet at <http://www.worldscinet.com/jpp/jpp.shtml>. Crystallographic data have been deposited at the Cambridge Crystallographic Data Centre (CCDC) under number CCDC-1943641 (nickel(II) porphyrin **2-trans**). Copies can be obtained on request, free of charge, via [http://www.ccdc.cam.ac.uk/data\\_request/cif](http://www.ccdc.cam.ac.uk/data_request/cif) or from the Cambridge Crystallographic Data Centre, 12 Union Road, Cambridge CB2 1EZ, UK (fax: +44 1223-336-033 or email: [deposit@ccdc.cam.ac.uk](mailto:deposit@ccdc.cam.ac.uk)).

### REFERENCES

- Davis JT and Spada GP. *Chem. Soc. Rev.* 2007; **36**: 296–313.
- Doluca O, Withers JM and Filichev VV. *Chem. Rev.* 2013; **113**: 3044–3083.
- Bolchman ML, Paeschke K and Zakian VA. *Nat. Rev. Genet.* 2012; **13**: 770–780.
- Fritzsche W and Spindler L. *Guanine Quartets: Structure and Applications*, Royal Society of Chemistry: Cambridge, 2013.
- Xu Y, Ishizuka T, Kurabayashi K and Komiyama M. *Angew. Chem., Int. Ed.* 2009; **48**: 7833–7836.
- Rankin S, Reszka AP, Huppert J, Zloh M, Parkinson GN, Todd AK, Ladame S, Balasubramanian S and Neidle S. *J. Am. Chem. Soc.* 2005; **127**: 10584–10589.
- Neidle S. *FEBS J.* 2010; **277**: 3470–3488.
- Monchaud D and Teulade-Fichou MP. *Org. Biomol. Chem.* 2008; **6**: 627–636.
- Collie GW and Parkinson GN. *Chem. Soc. Rev.* 2011; **40**: 5867–5892.
- Sabater L, Nicolau-Travers ML, De Rache A, Prado E, Dejeu J, Bombarde O, Lacroix J, Calsou P, Defrancq E, Mergny JL, Gomez D and Pratiel G. *J. Biol. Inorg. Chem.* 2015; **20**: 729–738.
- Bhattacharjee AJ, Ahluwalia K, Taylor S, Jin O, Nicoludis JM, Buscaglia R, Chaires B, Kornfilt DJP, Marquardt DGS and Yatsunyk LA. *Biochimie* 2011; **93**: 1297–1309.
- Romera C, Bombarde O, Bonnet R, Gomez D, Dumy P, Calsou P, Gwan J-F, Lin J-H, Defrancq E and Pratiel G. *Biochimie* 2011; **93**: 1310–1317.
- Kim YH, Lee C, Kim SK and Jeoung SC. *Biophys. Chem.* 2014; **190**: 17–24.
- Gaier AJ and McMillin DR. *Inorg. Chem.* 2015; **54**: 4504–4511.
- Sabater L, Fang P-J, Chang C-F, De Rache A, Prado E, Dejeu J, Garofalo A, Lin J-H, Mergny J-L, Defrancq E and Pratiel G. *Dalton Trans.* 2015; **44**: 3701–3707.
- Siddiqui-Jain A, Grand CL, Bearss DJ and Hurley LH. *Proc. Natl. Acad. Sci. U. S. A.* 2002; **99**: 11593–11598.
- Guo K, Pourpak A, Beetz-Rogers K, Gokhale V, Sun D and Hurley LH. *J. Am. Chem. Soc.* 2007; **129**: 10220–10228.
- Freyer MW, Buscaglia R, Kaplan K, Cashman D, Hurley LH and Lewis EA. *Biophys. J.* 2007; **92**: 2007–2015.
- Shi DF, Wheelhouse RT, Sun D and Hurley LH. *J. Med. Chem.* 2001; **44**: 4509–4523.
- Lefebvre JF, Leclercq D, Gisselbrecht JP and Richeter S. *Eur. J. Org. Chem.* 2010; 1912–1920.
- Lo M, Lefebvre JF, Leclercq D, van der Lee A and Richeter S. *Org. Lett.* 2011; **13**: 3110–3113.
- Rubio-Magnieto J, Di Meo F, Lo M, Delcourt C, Clément S, Norman P, Richeter S, Linares M and Surin M. *Org. Biomol. Chem.* 2015; **13**: 2453–2463.
- Schindler, J, Kupfer S, Ryan AA, Flanagan KJ, Senge MO and Dietzek B. *Coord. Chem. Rev.* 2018; **36**: 1–16.
- Senge MO and Kalisch WW. *Inorg. Chem.* 1997; **36**: 6103–6116.
- Wang Y and Patel DJ. *Structure* 1993; **1**: 263–282.
- Dai J, Carver M and Yang D. *Biochimie* 2008; **90**: 1172–1183.
- Bončina M, Lah J, Prislán I and Vesnaver G. *J. Am. Chem. Soc.* 2012; **134**: 9657–9663.
- Ambrus A, Chen D, Dai J, Bialis T, Jones RA and Yang D. *Nucleic Acids Res.* 2006; **34**: 2723–2735.
- Dai J, Punchihewa C, Ambrus A, Chen D, Jones RA and Yang D. *Nucleic Acids Res.* 2007; **35**: 2440–2450.
- Allenmark S. *Chirality* 2003; **15**: 409–422.
- Zhao P, Lu JZ, Hong FY, Ou BH, Zhang F, Ma L and Guo H. *Spectrochim. Acta, Part A* 2013; **108**: 1–7.

32. Pan J and Zhang S. *J. Biol. Inorg. Chem.* 2009; **14**: 401–407.
33. Lubitz I, Borovok N and Kotlyar A. *Biochemistry* 2007; **46**: 12925–12929.
34. Balaz M, De Napoli M, Holmes AE, Mammana A, Nakanishi K, Berova N and Purrello R. *Angew. Chem., Int. Ed.* 2005; **44**: 4006–4009.
35. Balaz M, Bitsch-Jensen K, Mammana A, Ellestad GA, Nakanishi K and Berova N. *Pure Appl. Chem.* 2007; **79**: 801–809.
36. De Cian A, Guittat L, Kaiser M, Saccà B, Amrane S, Bourdoncle A, Alberti P, Teulade-Fichou MP, Lacroix L and Mergny JL. *Methods* 2007; **42**: 183–195.
37. Renčiuk D, Zhou J, Beaupaire L, Guédin A, Bourdoncle A and Mergny JL. *Methods* 2012; **57**: 122–128.
38. CrysAlisPro Rigaku Oxford Diffraction Technologies, England 2012.
39. van der Lee A. *J. Appl. Crystallogr.* 2013; **46**: 1306–1315.
40. Palatinus L and Chapis G. *J. Appl. Crystallogr.* 2007; **40**: 786–790.
41. Betteridge PW, Carruthers JR, Cooper RI, Prout K and Watkin DJ. *J. Appl. Crystallogr.* 2003; **36**: 1487–1487.